ACS APPLIED MATERIALS & INTERFACES

Research Article

www.acsami.org

Structurally Driven Enhancement of Resonant Tunneling and Nanomechanical Properties in Diamond-like Carbon Superlattices

Neeraj Dwivedi,*[,†,‡,§] Ross McIntosh,[‖] Chetna Dhand,[‡,⊥] Sushil Kumar,*[,‡] Hitendra K. Malik,[§] and Somnath Bhattacharyya*[,‖]

[†]Department of Electrical and Computer Engineering, National University of Singapore, Singapore 117583, Singapore

[‡]CSIR-National Physical Laboratory, K.S. Krishnan Road, New Delhi 110012, India

[§]Department of Physics, Indian Institute of Technology Delhi, New Delhi 110016, India

[‖]Nano-Scale Transport Physics Laboratory, School of Physics, and Centre of Excellence in Strong Materials, University of the Witwatersrand, Private Bag 3, WITS 2050 Johannesburg, South Africa

[⊥]Singapore Eye Research Institute, Singapore 169856, Singapore

Supporting Information

ABSTRACT: We report nitrogen-induced enhanced electron tunnel transport and improved nanomechanical properties in band gap-modulated nitrogen doped DLC (N-DLC) quantum superlattice (QSL) structures. The electrical characteristics of such superlattice devices revealed negative differential resistance (NDR) behavior. The interpretation of these measurements is supported by 1D tight binding calculations of disordered superlattice structures (chains), which include bond alternation in sp^3-hybridized regions. Tandem theoretical and experimental analysis shows improved tunnel transport, which can be ascribed to nitrogen-driven structural modification of the N-DLC QSL structures, especially the increased sp^2 clustering that provides additional conduction paths throughout the network. The introduction of nitrogen also improved the nanomechanical properties, resulting in enhanced elastic recovery, hardness, and elastic modulus, which is unusual but is most likely due to the onset of cross-linking of the network. Moreover, the materials' stress of N-DLC QSL structures was reduced with the nitrogen doping. In general, the combination of enhanced electron tunnel transport and nanomechanical properties in N-DLC QSL structures/devices can open a platform for the development of a new class of cost-effective and mechanically robust advanced electronic devices for a wide range of applications.

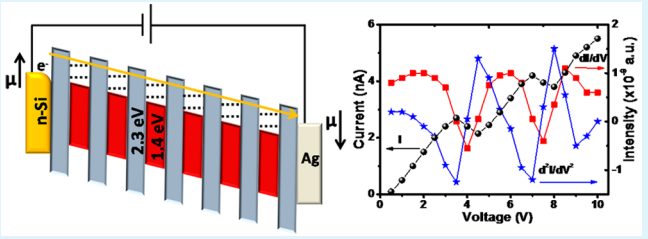

KEYWORDS: *superlattice, carbon, resonant tunneling, hardness, elastic recovery*

1. INTRODUCTION

Superlattice structures demonstrate quantum transport and tunable electronic characteristics, which can be utilized for the development of fast and efficient electronic, optoelectronic, and luminescent devices. Superlattices show unusual electrical transport, that is, homogeneous and inhomogeneous field-dependent transport. At a certain field (voltage), known as critical field (voltage), these structures exhibit negative differential conductance (NDC), alternatively called negative differential resistance (NDR). Superlattice structures have many interesting applications such as in high frequency electronics usually in oscillators, switching devices, memristors, programmable logic, computing, light emitting diodes, etc.

The idea of superlattice devices was proposed and executed by Tsu, Esaki, and Chang[1,2] while studying quantum devices based on lattice matched crystalline semiconductors. However, if the lattice constants of two semiconductors in crystalline superlattices are not perfectly matched, dislocations due to the misfit are generated leading to a high defect density. This results in strong electron scattering, restricting quantum effects. Thus, electron scattering has been a major hindrance to the realization of quantum effects in crystalline superlattices. In 1983, Abeles and Tiedje[3] suggested amorphous semiconductors could circumvent these detrimental interfacial effects. While studying a-$Si_{1-x}N_x$:H/a-Si:H and a-Ge:H/a-Si:H heterostructures, they also demonstrated the appearance of quantum size effects in amorphous superlattices. The amorphous structure of these superlattices relaxed the lattice matching condition of crystalline superlattices, while the hydrogen passivated defects and reduced the defect density, finally minimizing the electron scattering and allowing quantum effects to be observed. Hence, a-Si:H-based quantum superlattice (QSL) structures have been more widely studied than other amorphous QSL structures.[3]

The promise of extending these capabilities prompted the study of amorphous carbon devices. With the flexibility of tailoring the band gap over a wide range, ∼1−4 eV, coupled with tunable electronic properties, high thermal conductivity, and high wear resistance (10 000 times greater than a-Si:H),

Received: June 25, 2015
Accepted: September 7, 2015
Published: September 7, 2015

DOI: 10.1021/acsami.5b05657
ACS Appl. Mater. Interfaces 2015, 7, 20726−20735

hydrogenated amorphous carbon (a-C:H) or diamond-like carbon (DLC) provides a potential candidate for developing a new class of mechanically robust quantum electronic devcies.[4−14] Moreover, as it can be deposited over wide areas at low temperatures (usually room temperature), DLC can be deposited on inexpensive substrates, which is commercially important for evolving cost-effective technology. Utilizing its tunable optical and electronic characteristics, Silva et al.[15] demonstrated quantum size effects in DLC-based amorphous superlattice structures comprised of very thin low and high band gap DLC layers. The current−voltage (I−V) characteristics of the DLC-based superlattice structures revealed NDR features with the variation of current in the range 0.1−0.3 nA upon increasing the voltage to ∼6 V.[15] Subsequently, the structure of individual layers of DLC in superlattices was studied through transmission electron microscopy.[16] Bhattacharyya et al.[17] demonstrated resonant tunneling (NDR) and fast switching in DLC-based quantum well structures, which was a major effort toward realizing DLC-based fast quantum electronic devices.

Although DLC films have the capability of demonstrating quantum size effects, applications of these devices were limited due to low conductivity. Moreover, DLC films show high residual stress that may lead to poor adhesion of the films to the underlying substrate. Nitrogen has proven to be the best doping material for DLC to improve its electron transport and to reduce the stress.[4,6,10,18] Silva et al.[6] and Schwan et al.[10] have realized a significant improvement in the conductivity with a reduction in material stress of DLC films based on the introduction of nitrogen. In terms of devices, recently Katkov and Bhattacharyya[19] proposed a theoretical model for enhancing the tunnel transport in disordered carbon superlattice structures through the addition of nitrogen.

In view of the above, investigating and understanding the tunnel transport and nanomechanical properties of nitrogen doped DLC (N-DLC) QSL structures would be quite important from both scientific and technological perspectives. Thus, probing the role of nitrogen inclusion on the structural, nanomechanical, and tunnel transport properties of N-DLC QSL structures lies at the core of this study. In the present work, we have been able to improve electron tunnel transport in such structures by introducing nitrogen and controlling the microstructure. On the basis of this work, a fundamental understanding is also developed for the enhanced electron tunnel transport due to nitrogen doping, and its role in the stress and nanomechanical properties of N-DLC QSL structures.

2. MATERIALS AND METHODS

We study three QSL structures where the only difference is the nitrogen partial pressure (NPP) in the growth chamber to illustrate the positive effect of nitrogen inclusion on the structural and electronic and nanomechanical properties of the QSL structures, rather than systematically quantify the change in the properties. Band gap modulated N-DLC QSL structures were deposited at room temperature, on well cleaned Si ⟨100⟩ and Corning 7059 glass substrates at base and working pressures of 5×10^{-6} Torr and 25 mTorr, respectively, using asymmetric capacitive coupled radio frequency-plasma enhanced chemical vapor deposition (RF-PECVD). The acetylene (C_2H_2) and nitrogen (N_2) were used as precursor gases. Before the deposition of the final N-DLC QSL structures, the deposition rate at negative self-bias of 100 and 350 V for the films grown at NPP of 0% was calibrated. Once the calibration of deposition rate had been performed, the final N-DLC QSL structure was deposited at NPP of 0%, where NPP = $N_2/(N_2 + C_2H_2)$. By synchronizing the deposition time based on the calibrated deposition rate at NPP of 0%, 7 high band gap layers (each ∼3.5 nm thick) and 6 low band gap layers (each ∼2.5 nm thick) were deposited, alternatively. Following the same strategy, the deposition of N-DLC QSL structures at NPPs of 48.3% and 65.2% was carried out whereby the deposition time for the biases 100 and 350 V was kept the same as used in the case of 0% NPP. However, due to the addition of nitrogen, the total thicknesses and hence the deposition rate of N-DLC QSL structures were found to be slightly decreased at NPPs of 48.3% and 65.2%. The deposition rate for these N-DLC QSL structures was measured ex situ. Thus, each of these QSL structures consists of 7 high band gap and 6 low band gap layers, which enable 6 wells and 7 barriers in the structure. The high band gap layer was deposited at negative self-bias of 100 V, and the low band gap layer was grown at negative self-bias of 350 V.

The optical properties were measured using a UV−vis−NIR spectrophotometer (model 2200DPCV, Phoenix). FTIR measurements were carried out with a PerkinElmer Spectrum Bx instrument. The Raman spectra were recorded using a Renishaw InVia micro-Raman spectrophotometer. Visible light of wavelength 514.5 nm was used as an excitation source. The residual stress was estimated by change in the radius of curvature before and after deposition using a 500TC temperature controlled film stress measurement system (FSM Frontier Semiconductor, U.S.). The residual stress (S) was calculated using the Stoney eq 1:

$$S = \frac{E_s d_s^{\,2}}{6(1-\nu_s)d_f}\left(\frac{1}{R_f} - \frac{1}{R_0}\right) \tag{1}$$

where E_s, ν_s, d_f, and d_s are Young's modulus, the Poisson ratio, the film thickness, and thickness of substrate, respectively, and R_0 and R_f are the radii of substrate curvature before and after the film deposition. The nanomechanical properties were determined using fully automatic software controlled IBIS nanoindentation (Fisher-Cripps laboratories Pvt., Australia) with a triangular pyramid diamond Berkovich indenter. The maximum indentation load in all of the measurements was kept at 300 μN. Ten indentations were made on each sample, and average values of the hardness and elastic modulus are reported. I−V characteristics were recorded at room temperature in a sandwiched configuration using Keithley 6487 Pico Ammeter instrument.

We employ a 1D tight-binding model to calculate the transport properties of nitrogen incorporated DLC superlattice structures. The tight-binding model is given by eq 2:

$$\mathcal{H} = \sum_i \varepsilon_i c_i^{\dagger} c_i - \sum_{\langle i,j \rangle} t_{i,j}(c_i^{\dagger} c_j + c_j^{\dagger} c_i) \tag{2}$$

where ε_i is the on-site energy, $c_i^{\dagger}$ and c_i are the Fermion creation and annihilation operators, and $t_{i,j}$ represents the tight-binding hopping parameter while the summation is taken over nearest neighbor sites. Although devices are made of 2D layers, the contacts are perpendicular to the layers so current propagates through 1D or quasi-1D channels.

The sp^3-hybridized regions have a relatively high potential (corresponding to a relatively small hopping parameter) forming potential barriers, while the potential in the sp^2-hybridized regions is lower (corresponding to a relatively large hopping parameter) forming quantum wells. Structural disorder in the form of bond-length distortions is modeled by using a nonuniform distribution of the tight-binding hopping parameter, which follows a Gaussian distribution about a mean value. The width of this distribution is referred to as the disorder parameter. The structural bond length distortion is related to a change in the tight binding hopping parameter via a bond deformation potential.[20] The hopping parameter and the disorder parameter used in this work were determined through a combination of previous theoretical and experimental studies.[21] Details can be found in our previous studies.[19,22,23]

The discretized Schrödinger eq 3:

$$E\Psi_i = \varepsilon_i \Psi_i - t_{i+1,i}\Psi_{i+1} - t_{i-1,i}\Psi_{i-1} \tag{3}$$

DOI: 10.1021/acsami.5b05657
ACS Appl. Mater. Interfaces 2015, 7, 20726−20735

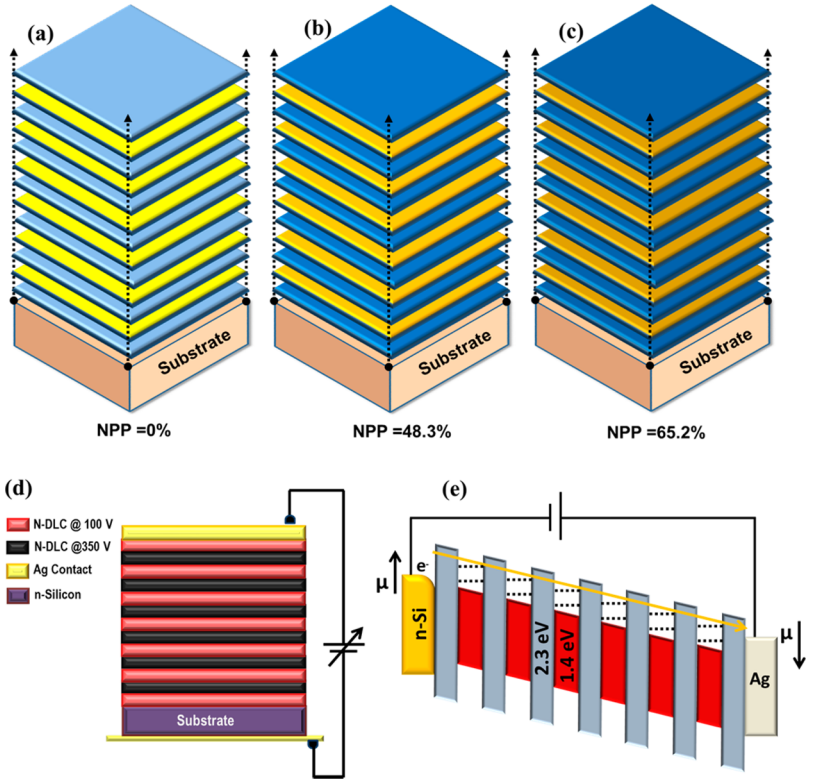

Figure 1. Schematic representation of N-DLC QSL structures and devices. These N-DLC QSL structures were deposited at NPPs of (a) 0%, (b) 48.3%, and (c) 65.2%. Each N-DLC QSL structure comprises 7 wide band gap layers (represented by dark blue and light blue colors) and 6 low band gap layers (represented by yellow and orange colors). (d) For the electrical measurements, Ag contacts were made at the front and at the back of the QSL structures and (e) N-DLC QSL device under bias illustrating resonant tunneling where μ is the chemical potential of the leads.

was solved iteratively using the known eigenvalue for $E = E_L - 2t_L \cos(k_L)$, the left lead, where E_L is the on-site energy in the left lead with hopping parameter t_L and incident wavevector k_L. The transmission coefficient was defined as $T(E) = (\sin(k_L)/|A|^2 \sin(k_R))$, where k_L is the wavevector of the incoming wave from the left lead, k_R is the wavevector of the right lead, and A is the incoming wave amplitude. The current−voltage characteristics were then calculated from the transmission coefficient using the Landauer−Büttiker formula.

We studied two different cases theoretically. Initially, we studied the transmission through disordered superlattices, which are similar to conventional superlattice structures, that is, regions of high potential separated by regions of low potential. The eigenenergies are sensitive to the relative difference in potential between the quantum wells and barriers. Consequently, the regions where NDR is found in the $I-V$ characteristics can be tuned. However, the separation of the regions of NDR cannot be tuned to reproduce the experimental data using physical parameters for the potential as the eigenenergies of the superlattice are relatively close together while the experimental data show a large difference in the potential between the regions of NDR. This prompted us to study the case of bond alternation in the sp^3-hybridized regions, which is likely to arise if polymeric chains form within the sp^3-hybridized regions. The periodic bond alternation in the sp^3-hybridized regions results in alternation of the hopping parameter, which varies from one site to the next, from t^{max}_{σ} to t^{min}_{σ}, which are in the range of 3.3−4.3 and 1.1−2.1 eV, respectively, with the transfer hopping parameter between the diamond-like and graphitic regions given by $t_{\sigma-\pi}$, which is 1.37 eV.[19,23] There may also be significant incorporation of sp^2C in the sp^3-hybridized regions as well as incorporation of nitrogen complexes in the sp^3-hybridized regions. However, the effects of these inclusions will be similar to bond alternation as they result in a much smaller potential locally in the sp^3-hybridized regions. Hence, we neglect to model defects of this form. There may also be disorder within the bond alternation regions, although this has a relatively small effect on the transmission coefficient as the relative change in the potential across the sites due to disorder is quite small in comparison with the change in potential from site to site due to bond alternation.

It was difficult to quantitatively reproduce the experimental data as nitrogen can from a number of different C−N complexes (with different potentials) and can modify the microstructure in the region of the nitrogen defect.[22] Networks, sp^2 clusters, and polymeric chains can form in the DLC superlattices. In this work, we have considered uniform nitrogen defects, although it is possible that different nitrogen-related defects are incorporated in the sp^2C regions. Calculations of the $I-V$ characteristics allow us to interpret general features of the measurements on the basis of a well-established quantum transport treatment.

3. RESULTS AND DISCUSSION

Superlattice structures are composed of periodic arrays of barriers and wells. In band gap-modulated superlattice structures, a single barrier is formed when a thin semiconducting layer of wide band gap material is sandwiched between two narrow band gap layers. Similarly, a well is formed when a low band gap layer is sandwiched between two wide band gap layers. So the array of alternating wide and low band gap layers constructs the array of quantum wells and barriers. These heterostructures are known as superlattice structures. However, if the thickness of these layers is very small (well within the coherence length), that is, in the range of a few nanometers, quantum effects may be observed. Under such conditions, a superlattice is called a QSL. It is important to mention that QSL structures maintain the periodicity, and besides crystalline materials, these structures can also be prepared using amorphous semiconducting materials.

DOI: 10.1021/acsami.5b05657
ACS Appl. Mater. Interfaces 2015, 7, 20726−20735

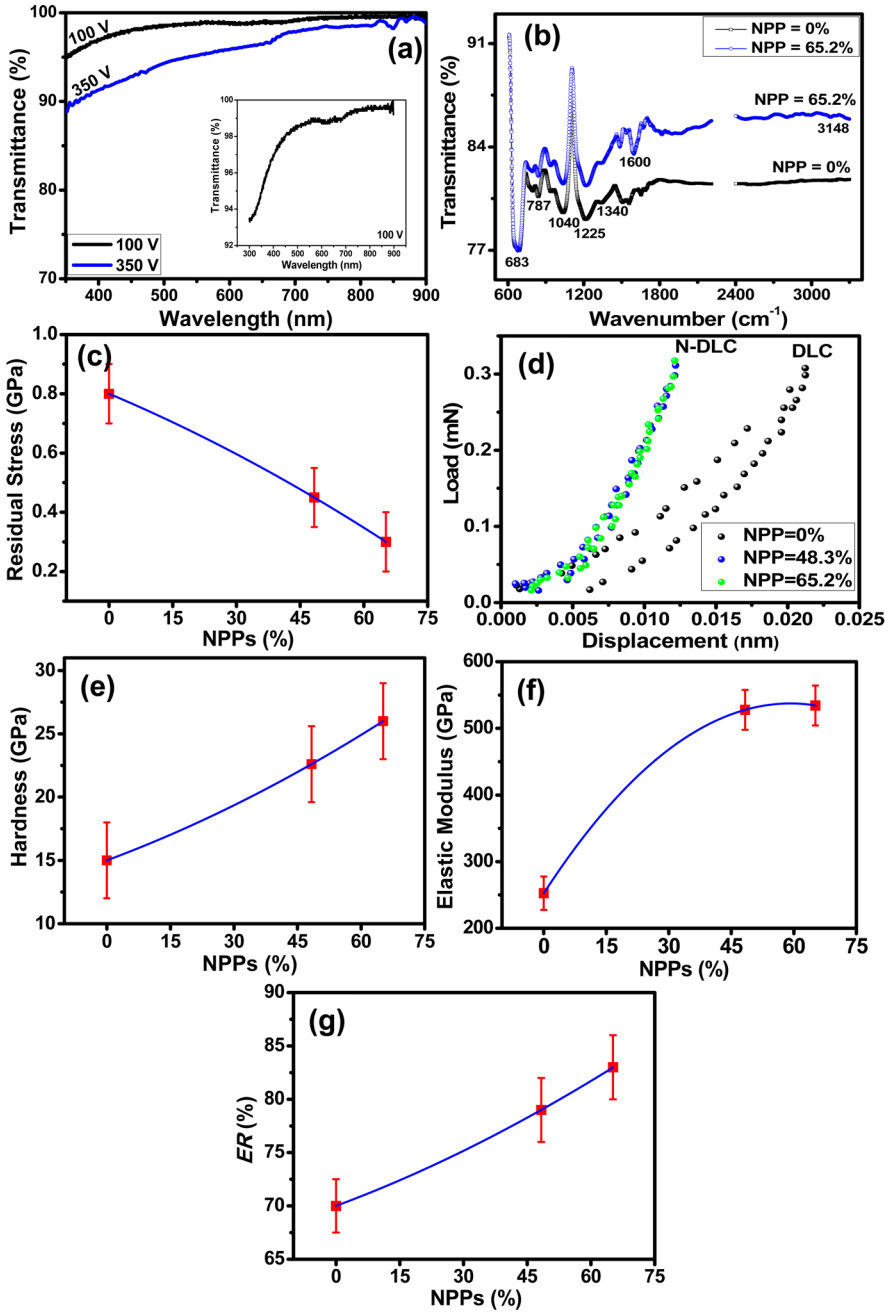

Figure 2. Spectroscopic (UV−vis−NIR and FTIR) analyses, residual stress, and nanomechanical properties. (a)Transmittance spectrum of a single DLC layer deposited at 0% NPP and at negative self-bias of 100 and 350 V. Inset of (a) shows the zoomed-in version of transmittance for 100 V grown film. (b) Fourier transform infrared (FTIR) spectra of N-DLC QSL structures deposited at NPP of 0% and 65.2%. Variations of (c) residual stress, (e) hardness, (f) elastic modulus, and (g) elastic recovery with NPPs and (d) load versus displacement curves for N-DLC QSL structures. The blue line shows the polynomial fitting of the graph points.

The N-DLC QSL structures were fabricated precisely with varying nitrogen partial pressures (NPPs) of 0%, 48.3%, and 65.2%. In QSL structures, wide band gap layers were grown at negative self-bias of 100 V, whereas low bad gap layers were deposited at 350 V. Each N-DLC QSL structure comprises 7 high band gap layers and 6 low band gap layers deposited alternatively (schematically shown in Figure 1a−c).

Similar to Abeles and Tiedje,[3] the thickness of the layers was controlled and determined by the deposition rate. The total thickness of the N-DLC QSL structures comprising 7 high band gap layers (barriers) and 6 low band gap layers (wells) at NPP of 0%, 48.3%, and 65.2% was found to be ∼40, ∼36, and ∼30 nm, respectively. The deposition rates were found to be 0.26, 0.23, and 0.20 nm/s, respectively.

For the N-DLC QSL structure grown at NPP of 0%, the barrier layer has a thickness of ∼3.5 nm and the well layer has a thickness of ∼2.5 nm. Because the deposition rate and hence overall the thickness of the N-DLC QSL structures were decreased with increasing NPPs, the N-DLC structures deposited at NPPs of 48.3% and 65.2% would have slightly reduced barrier and well thickness. The decrease of deposition rate means there is a competition between deposition and etching of the film due to ionic bombardment (nitrogen ions) on the growing film surface.[24] The increase in NPP also

DOI: 10.1021/acsami.5b05657
ACS Appl. Mater. Interfaces 2015, 7, 20726−20735

suppresses the transport of carbon species with nitrogen, reducing the deposition rate.

The transmittance spectra of an individual layer of N-DLC films grown at 0% NPP (pure DLC) and at negative self-bias of 100 and 350 V, taken by ultraviolet−visible−near-infrared (UV−vis−NIR) spectroscopy, are shown in Figure 2a. Because the individual layers were extremely thin, their transmittance was found to be very high, which varied in the range ∼95−99.5% (for 100 V grown film) and ∼90−99% (for 350 V grown film) with increasing wavelength from 350 to 900 nm. The transmittance spectra of the film grown at 100 V showed slightly higher optical transparency than the one grown at 350 V, which may be due to the occurrence of relatively higher diamond-like character (slightly higher band gap) in the former film. The optical band gap of a single layer N-DLC film grown at 0% NPP was estimated by the Tauc method[25,26] and found to be 2.3 eV at 100 V and 1.4 eV at 350 V. The high band gap at 100 V is attributed to the formation of more diamond-like structure, and the low band gap at 350 V corresponds to the reduction of sp^3C bonding and greater formation of the sp^2C phase and sp^2 clusters due to the relaxation process as described by Robertson for DLC films.[9] The high and low band gap layers, alternatively, enabled the band gap modulated N-DLC QSL structures.

Fourier transform infrared (FTIR) spectra of N-DLC QSL structures deposited at NPPs of 0% and 65.2% are shown in Figure 2b. A CO_2 peak due to atmospheric contamination was observed in these QSL structures. As this peak has no physical significance in relation to the properties of interest, the region 2200−2400 cm^{-1} was omitted from the FTIR spectra. Because the thickness of N-DLC QSL structures was low, various bonding states of Si with C, N, and H were seen in the spectra. The band in the range 620−733 cm^{-1} may be assigned to strong Si−C, Si−Si, and Si−N bonding. The region in the range 775−835 cm^{-1} may correspond to Si−CH_3 rocking modes probably containing strong Si−C interactions. The band in the 1000−1250 cm^{-1} range is assigned to the symmetric bending mode of CH_3 attached to Si. The vibrational bands observed near 1300−1350 cm^{-1} correspond to sp^3 (C−H) and sp^2 (C−H or C−C) bonding. Our primary interest is in the band range of 1550−1600 cm^{-1} as it corresponds to C═C bonding only. This band for a N-DLC QSL structure grown at NPP of 0% is ascribed to the presence of graphite-like sp^2 C═C vibrations, whereas for a N-DLC QSL structure grown at NPP of 65.2%, this corresponds to the existence of amino C═N groups. It should be noted that when the NPP is increased, the peak at 1550−1600 cm^{-1} becomes slightly more intense due to symmetry breaking caused by nitrogen introduction. This shows that the introduction of nitrogen enhances the sp^2 clustering and promotes the sp^2 phase as well. Wang et al.[27] have also observed similar behavior in hydrogenated amorphous carbon films and reported an enhancement in the intensity of the peak near 1600 cm^{-1} after nitrogen doping. This is explained by nitrogen-induced structural curvature of the carbon network. Peaks in the 3200−3500 cm^{-1} range may be assigned to N−H and O−H bonding. The FTIR results of these samples are in good agreement with the reported literature.[9,27−31] It is important to mention that the C−H stretching vibration band in the range 2700−3200 cm^{-1} was very faint in both of the structures. This indicates that these N-DLC QSL structures contain very little hydrogen. Raman measurements were also performed to further examine the microstructure of DLC films, which are discussed in the Supporting Information (S1). Raman results indicate that the introduction of nitrogen in DLC promotes sp^2 cluster formation, which is in good agreement with the FTIR spectra. We also observed that the size of the sp^2 clusters increased with increasing NPP due to the higher concentration of nitrogen in N-DLC QSL structures. In addition, the introduction of nitrogen seems to slightly increase (reduce) the overall sp^2 (sp^3) carbon bonding.

High residual stress is one of the most technically challenging difficulties to overcome in growing DLC films as high stress reduces the adhesion of DLC with the underlying substrate and can cause instant delamination.[32,33] However, the generation of high compressive stress is one of the mechanisms proposed for the growth of high sp^3 bonded DLC films.[34] Ferrari et al.,[35] on the other hand, suggested that it is not only the stress that influences the sp^3carbon bonding and vice versa but also that stress can be manipulated by rearranging the sp^2C phase. In this context, we discuss the role of nitrogen incorporation on the compressive stress of N-DLC QSL structures through Figure 2c. Unlike undoped DLC films, N-DLC QSL structures showed significantly lower material stress (below 1 GPa, maximum 0.8 GPa). Interestingly, a reduction of about 62% in the stress was encountered when the NPP was increased from 0% to 65.2%. The decrease of stress with increased NPP can be due to rearrangement of the sp^2carbon phase in terms of the increased number and size of sp^2 clusters, and overall sp^2C phase as evidenced by FTIR and Raman analyses. In addition, reduction of the average coordination number (nitrogen and carbon have coordination numbers of 3 and 4, respectively) and, hence, degree of overconstraining due to nitrogen introduction could be another reason for the reduction of stress.[36] Importantly, N-DLC QSL structures consist of high and low band gap layers. The low band gap layer grown at 350 V shows greater sp^2C bonding and acts as an adhesive layer to the subsequent high band gap layer having more sp^3C bonding. In this way, the presence of higher self-bias grown low band gap layers provides relaxation to the overall N-DLC QSL structure and hence reduces the stress.

The nanomechanical properties of N-DLC QSL structures, especially the hardness (H) and elastic modulus (E), were measured using nanoindentation at a load of 300 μN. Load versus displacement (LD) curves of N-DLC QSL structures are shown in Figure 2d, where the depth of penetration was found to decrease with increasing NPPs. This seems to be due to nitrogen-induced hardening of the N-DLC QSL structures. To estimate the hardness and elastic modulus, we analyze the LD curves. Because the penetration depth is higher than 10% of the total thickness of N-DLC QSL structures, H is determined by a composite hardness model.[37] Figure 2e and f shows the variations of H and E with NPP for N-DLC QSL structures. The values of H at NPPs of 0%, 48.3%, and 65.2% were found to be 15, 22.6, and 26 GPa, respectively. The values of E follow a similar trend and were found to increase from 252 to 534 GPa upon increasing the NPP from 0% to 65.2%. The elastic recovery (ER) of these samples was also determined (Figure 2g) using eq 4:

$$\%ER = \frac{(h_{max} - h_{res})}{h_{max}} \times 100 \quad (4)$$

where h_{max} and h_{res} are the displacement at the maximum load and residual displacement after load removal, respectively. The

DOI: 10.1021/acsami.5b05657
ACS Appl. Mater. Interfaces 2015, 7, 20726−20735

values of *ER* with the inclusion of NPP were found to be 70%, 79%, and 83%, respectively.

Usually the hardness of DLC films is inversely (direct) proportion to sp^2 (sp^3)carbon bonding. However, sp^2carbon bonding in N-DLC QSL structures seems to be slightly increased with the introduction of nitrogen, which indicates that other mechanism(s) is(are) governing the nanomechanical properties of N-DLC QSL structures. The nitrogen-induced onset of cross-linking of the carbon network[27,38−45]or formation of hard β-C_3N_4 phase[46,47] may be the possible mechanism(s) for improved nanomechanical properties of N-DLC QSL structures. It should be noted that, although the generation of the hard β-C_3N_4 phase has been predicted theoretically, practical realization of this phase is still under debate. The formation of β-C_3N_4 might be possible in highly energetic deposition processes such as in ion beam deposition or pulse laser deposition of carbon nitride films.[48] Hence, we neglect the formation of β-C_3N_4 phase in our PECVD deposited films.

While investigating the *ER* of these samples, we observed that it is significantly enhanced with the introduction of nitrogen. Previously, it was suggested that cross-linked carbon networks contribute to the enhancement of the *ER* and *H* of carbon films.[27,38−45] For PECVD grown hydrogenated carbon films, Wang et al.[41] observed *ER* (*H*) as high as 74% (8 GPa) in pure a-C:H films, which was increased to 84% (26 GPa) in a-C:H films with cross-linked carbon networks. In another work, Wang et al.[42] reported *ER* of 65% in pure a-C:H film, which was raised to 77−85% in a-C:H films with cross-linked carbon network. The role of nitrogen has been found to be very crucial in forming cross-linked carbon networks and sp^2 clusters for both the PECVD and sputtered amorphous carbon films.[27,43−45] For nitrogen doped sputtered carbon films, Hellegren et al.[43] have realized *ER* (*H*) of 75% (20 GPa) and 90% (40−60 GPa) in purely amorphous nitrogenated carbon films and amorphous nitrogenated carbon films with cross-linked carbon networks, respectively. Similarly, Wang et al.[27] realized an *ER* of 60% in PECVD deposited pure a-C:H films, which was increased to 75% in nitrogen doped a-C:H:N films, which have nitrogen-induced cross-linked carbon networks.[27]

In view of the established literature, we also predict that the introduction of nitrogen can lead to the onset of cross-linked carbon networks, which can therefore improve the elastic and nanomechanical properties of N-DLC QSL structures. For N-DLC QSL structures grown at 0% NPP (without nitrogen incorporation), in our case the *ER* is found to be lower due to the formation of an amorphous a-C:H film. However, it is enhanced to 79% and 83% in N-DLC QSL structures grown at NPPs of 48.3% and 65.2%, respectively, due to the formation of a-C:H:N films with some cross-linked network. To understand nitrogen-driven cross-linking, Sjostrom et al.[44] have carried out theoretical total energy calculations and proposed that an energy of 73.8 kcal/mol is required to form a cross-linked carbon network. However, the energy cost can be reduced by an amount of 26.2 kcal/mol, if two carbon atoms are replaced by nitrogen atoms in a cross-linked pentagonal network. In the present work, the deposition of N-DLC QSL structures is performed with two different self-biases of 100 and 350 V. Under biased conditions, Ar^+ ions present in the mixture of Ar−C_2H_2 plasma bombard the carbon species on the Si substrate and locally alter the thermodynamic relations, raising the local temperature. At the same time, the introduction of nitrogen in plasma affects the plasma chemistry and kinetics and alters the microstructure of films in the condensed state in terms of the formation of cross-linked networks in the matrix of amorphous carbon. Moreover, Hellgren et al.[43] have suggested that a high nitrogen concentration, which is a function NPP, promotes the generation of pentagons or curved structures even if the energy supplied is not sufficient. Hence, the onset of a nitrogen-induced cross-linked network is perhaps the reason for enhanced *ER* and *H* of N-DLC QSL structures.

Electrical transport through periodic structures has always been a subject of great interest. Periodic structures show either miniband conduction or Wannier−Stark hopping conduction or resonant sequential tunneling. For amorphous superlattices, the wave functions of different quantum wells are thought to be weakly coupled, and resonant sequential tunneling is thought to be the most probable form of tunneling. Figure 1d shows a schematic cross-sectional view of N-DLC QSL devices, where the high and low band gap layers were grown at negative self-biases of 100 and 350 V, respectively. Silver (Ag) was used as metal contacts, and then-Si substrate acted as an electron injector. Figures 1e is the horizontal view of the device under a bias voltage. Figure 3a shows the current−voltage (*I*−*V*) characteristics and its first- and second-order derivative curves

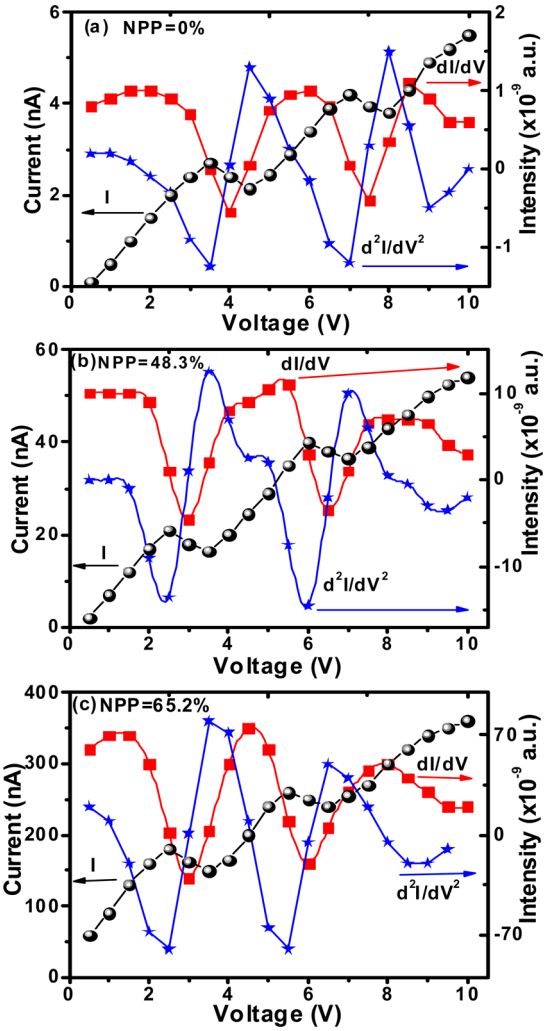

Figure 3. Electrical characteristics of N-DLC QSL structures at room temperature, showing NDR behavior. The *I*−*V* curve, the first-order derivative (dI/dV), and the second derivative (d^2I/dV^2) of N-DLC QSL structures deposited at NPP of (a) 0%, (b) 48.3%, and (c) 65.2%.

DOI: 10.1021/acsami.5b05657
ACS Appl. Mater. Interfaces 2015, 7, 20726−20735

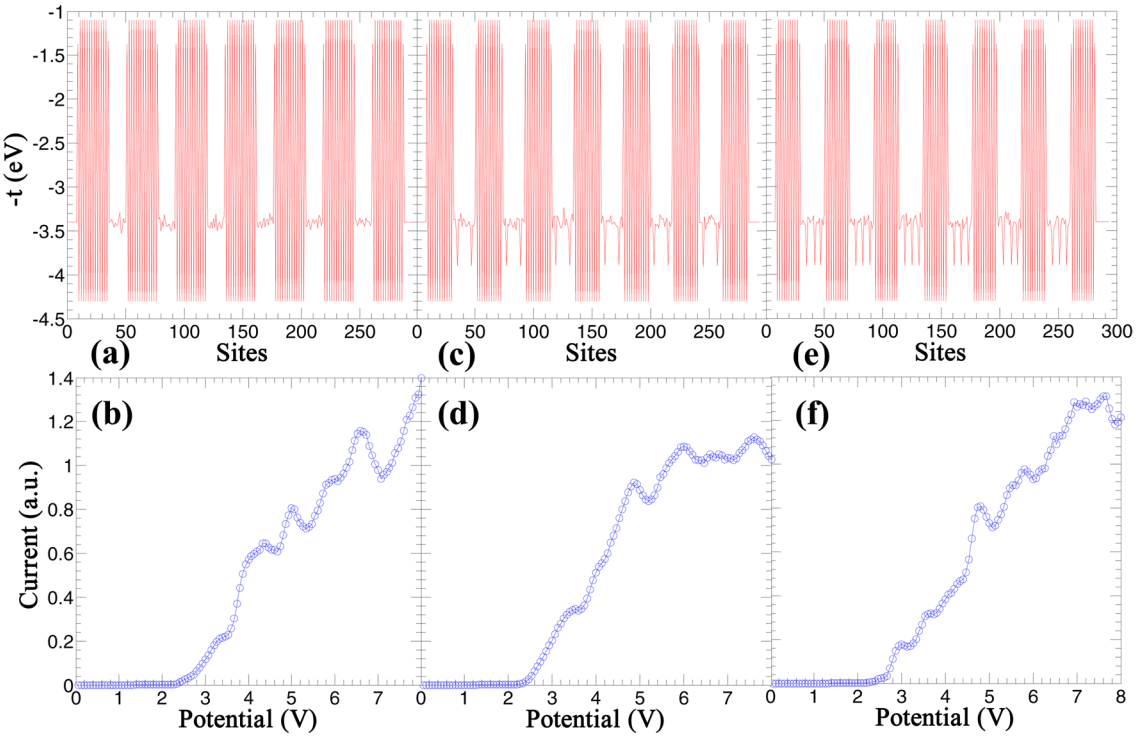

Figure 4. Calculated current−voltage characteristics and potential profile of disordered carbon superlattice structures with bond alternation in the sp^3-hybridized regions, with the same configuration as the experimental devices. (a) Structure with no nitrogen incorporation. (b) Current voltage characteristics of the structure with profile (a). (c) Structure with some nitrogen defects and reduced barrier width, (d) current−voltage characteristics of the structure (c). (e) Structure with still higher nitrogen defect concentration and further reduced barrier width, (f) calculated current−voltage characteristics of structure (e).

for a N-DLC QSL structure grown at 0% NPP (pure DLC QSL structure). The current was found to increase with increasing voltage and reached a local maximum value called the peak current. This is mainly due to the energy mismatch between the successive quantum wells, which confirms the sequentional resonant tunneling transport. This can be understood as follows: In the present case, we have 7 barriers (B_1, B_2, B_3, B_4, B_5, B_6, and B_7) and 6 wells (W_1, W_2, W_3, W_4, W_5, and W_6) (Figure 1e). Each well has different energy levels (say E_1, E_2, E_3, ...E_n). The first and seventh barriers are connected to electrodes, where n-Si acts as an electron injector.[17] When a potential difference is applied between the leads, the chemical potential decreases linearly throughout the superlattice from the high chemical potential of the source to the low chemical potential of the drain. When the potential difference of the leads causes the eigenenergies of the quantum wells to begin to align, the current begins to increase rapidly, and as resonant tunneling ensues, the current reaches a maximum. Subsequently, as the increasing potential destroys the alignment of the eigenenergies, the current decreases rapidly as resonant tunneling is suppressed, resulting in a decrease of current with voltage referred to as negative differential conductance (NDC) or negative differential resistance (NDR). Keay et al.[49] have observed NDR behavior in GaAs superlattice structures and suggested that it occurs due to alignment and misalignment of sub band states under applied voltage. For carbon-based materials, Bhattacharyya and Silva[50] have also found NDR behavior at room temprature for a-CN_x/Si heterostructures, which becomes prominent at 80 K.

The introduction of nitrogen in N-DLC QSL structures is found to modify the tunnel transport in terms of the change in NDR voltage(s) and total current. For the sample grown at 0% NPP, the peak currents are found at two discrete voltages of ∼3.5 and ∼7 V. When the NPP is increased to 48.3% (Figure 3b), the peak current and first and second NDR voltages shift toward lower values, 3 and 6.5 V, respectively. Moreover, the intensity of NDR (dI/dV) is increased with increasing NPP from 0% to 48.3%. When the NPP is further increased to 65.2% (Figure 3c), the first NDR peak remains at the same voltage (3 V) but the second NDR voltage shifts toward a lower value (6 V). In addition, the intensity of NDR is enhanced further for this sample. Thus, the NDR voltages shift successively toward lower values with the increasing NPPs. In addition, the total current of the devices is also increased by about 2 orders of magnitude with increasing NPPs from 0% to 65.2%. It should be noted that for all of the samples we found maxima in the current only at two discrete voltages despite having many wells and barriers, which is discussed subsequently during the discussion of theoretical results. Silva et al.[15] have also observed maximal current only at one voltage for DLC superlattice structures having multiple wells and barriers. Overall, the introduction of nitrogen in N-DLC QSL structures improves the electrical properties and nanomechanical properties. Hirono et al.[40] have also reported the coexistence of high electrical conductivity and superhard behavior in sp^2-rich carbon films due to the creation of carbon nanoparticles or cross-linking.

The non-hydrogenated amorphous carbon (a-C) films show a high degree of disorder. This high level of disorder may suppress the tunnel transport. However, in a-C:H films, the presence of hydrogen reduces the disorder by passivating the dangling bonds. The introduction of nitrogen in a-C:H can further enhance the tunnel transport in N-DLC due to the change in microstructure and bonding environment. In these N-DLC QSL structures, the increased sp^2 clustering, as

DOI: 10.1021/acsami.5b05657
ACS Appl. Mater. Interfaces 2015, 7, 20726−20735

evidenced by FTIR and Raman spectra, seems to be the main mechanism for the improved tunnel transport with the increased NPPs (or nitrogen).

To compare and understand the experimental results, that is, the enhanced electron tunnel transport with the introduction of nitrogen in N-DLC QSL structures, theoretical modeling was performed using a 1D tight-bonding model, as shown in Figures 4a–f. We assume that there is bond alternation in the sp^3-hybridized regions. This is discussed in the experimental section. Figure 4a shows the hopping parameter (inversely related to the potential) at each lattice site in the superlattice for a DLC QSL structure with the same dimensions as the experimentally studied N-DLC structure grown at 0% NPP (without nitrogen incorporation). Figure 4b shows the calculated $I-V$ characteristics. It was assumed that there is structural disorder within the sp^2C phase. There are two prominent regions of NDR, where the peaks are observed at 5 and 6.7 V as well as an additional peak at around 4 V and nonlinear features.

Reflection of the wave function from sp^3-hybridized regions results in quantum interference with constructive interference occurring at the eigenenergies, resulting in resonant transmission when the potential causes alignment of the eigenenergies of the quantum wells with the incident electron energies of the leads. The bond-alternation in the sp^3-hybridized regions increases the separation between the eigenenergies, shifting the eigenenergies closer to the band edges with increasing sp^3 percentage.[19] The bond-alternation also increases the transparency of the superlattice and increases the difference between the eigenenergies of the quantum wells as at high incident electron energies the barriers become more transparent to the incident electrons (for a solid barrier), and this effect is enhanced in the case of bond-alternation. The disorder in the sp^2C phase results in a wide distribution of eigenenergies, resulting in the broad transmission maxima and decreasing the peak-to-valley ratio in the $I-V$ characteristics.

With increasing nitrogen partial pressure during synthesis, the number of nitrogen atoms incorporated in carbon networks of N-DLC QSL structures significantly increases the number and size of sp^2 clusters as well as the overall sp^2/sp^3 ratio (as shown by FTIR and Raman measurements in this study and found in other studies as well). In modeling the nitrogen incorporated superlattice structures, we have included these effects. Because it is difficult to state with certainty the amount of nitrogen defects incorporated in the sp^2 carbon regions, we have included a few nitrogen atoms in these regions to qualitatively interpret the effects of nitrogen defect incorporation. Figure 4d shows the calculated current–voltage characteristics of a N-DLC QSL structure with nitrogen defects where the width of the sp^3-hybridized regions has been reduced in accordance with the experimentally observed increase in the size and number of sp^2 clusters and overall amount of the sp^2C phase (structure in Figure 4c). In agreement with the measurements, the regions of NDR shift toward lower potentials as the superlattice becomes more transparent with the decreasing sp^3C barrier thickness. The defects decrease the potential at which the first region of NDR occurs, while the potential of the second region of NDR shifts to the lower potential due to the increased transparency. In addition, higher-order regions of NDR become apparent due to the increased quantum well width. These do not appear in the measurements; however, they may be drowned out by multichannel effects as many conduction channels form in the DLC superlattice structures. The potential of the Si injector may also play a role in suppressing these regions.

Figure 4f shows the calculated $I-V$ characteristics for a nitrogen defect incorporated N-DLC QSL structure with a still greater defect concentration and further increase of sp^2 clusters (structure in Figure 4e). The first and second prominent regions of NDR shift to slightly smaller potentials, although the shift in potential is not as great as the initial shift when the nitrogen is first introduced, coinciding with the measurements. Between these regions additional nonlinear features are found, which indicate broad transmission maxima that are not sharp enough to induce NDR. The defect states result in additional eigenenergies forming in the quantum wells. The calculations allow us to interpret with certainty the effects of the nitrogen incorporation in the experimental data.

The experimental results show a marked increase in the conductivity with the increasing nitrogen incorporation, almost an order of magnitude with each increase in the nitrogen partial pressure. This is likely due to the formation of additional conduction channels (quasi-1D chains and networks) in the superlattice. These additional conducting channels correspond to the increased sp^2 clusters. The effect of multiple conduction channels and the incorporation of various nitrogen complexes accounts for most of the discrepancies between the measured and calculated $I-V$ characteristics. These calculations provide a convincing explanation of the experimental data and also yield insight on the design of DLC superlattice devices with specified characteristics.

4. CONCLUSION

Three band gap modulated N-DLC QSL structures with and without nitrogen introduction have been fabricated to uncover the effect of nitrogen incorporation on their electrical and nanomechanical properties. We observed quantum size effects in the N-DLC QSL structures in the form of resonant tunneling. The electrical properties revealed enhanced electron tunnel transport with the increasing NPPs, in agreement with the theoretical calculations conducted using a 1D tight-binding model. The NDR voltage consecutively shifted toward smaller potentials while the total current increased with increasing NPPs. We believe that the generation of nitrogen-induced additional 1D channels and networks, which arise as the number of sp^2 clusters increases, is the origin of the enhanced tunnel transport in N-DLC QSL structures. These N-DLC QSL structures also showed anomalous hardness and elastic recovery characteristics, which are most likely due to the onset of nitrogen-induced cross-linking of the carbon network, in agreement with the enhancement of the tunnel transport properties. This discovery can be extremely important toward the development of cost-effective and mechanically robust fast quantum electronic devices.

■ ASSOCIATED CONTENT

Supporting Information

The Supporting Information is available free of charge on the ACS Publications website at DOI: 10.1021/acsami.5b05657.

Raman spectroscopic analysis of N-DLC superlattice structures (PDF)

■ AUTHOR INFORMATION

Corresponding Authors

*E-mail: neerajdwivedi6@gmail.com, eleneer@nus.edu.sg.

DOI: 10.1021/acsami.5b05657
ACS Appl. Mater. Interfaces 2015, 7, 20726–20735

*E-mail: skumar@nplindia.org.
*E-mail: somnath.bhattacharyya@wits.ac.za.

Notes

The authors declare no competing financial interest.

■ ACKNOWLEDGMENTS

We are grateful to the Director, NPL New Delhi, for his kind support. We thank Prof C. S. Bhatia, National University of Singapore, Singapore, for fruitful discussions. We also thank M. V. Katkov for valuable discussions. S.B. would like to thank the National Research Foundation (SA) for granting the Nanotechnology flagship Programme to perform this work and also the University of the Witwatersrand Research Council for financial support.

■ REFERENCES

(1) Tsu, R.; Esaki, L. Tunneling in a Finite Superlattice. *Appl. Phys. Lett.* **1973**, *22*, 562−564.
(2) Esaki, L.; Chang, L. L. New Transport Phenomenon in a Semiconductor Superlattice. *Phys. Rev. Lett.* **1974**, *33*, 495−498.
(3) Abeles, B.; Tiedje, T. Amorphous Semiconductor Superlattices. *Phys. Rev. Lett.* **1983**, *51*, 2003−2006.
(4) Dwivedi, N.; Kumar, S.; Malik, H. K. Studies of Pure and Nitrogen Incorporated Hydrogenated Amorphous Carbon Thin Films and their Possible Application for Amorphous Silicon Solar Cells. *J. Appl. Phys.* **2012**, *111*, 014908.
(5) Dwivedi, N.; Kumar, S.; Carey, J. D.; Tripathi, R. K.; Malik, H. K.; Dalai, M. K. Influence of Silver Incorporation on the Structural and Electrical Properties of Diamond-like Carbon Thin Films. *ACS Appl. Mater. Interfaces* **2013**, *5*, 2725−2732.
(6) Silva, S. R. P.; Robertson, J.; Amaratunga, G. A. J.; Rafferty, B.; Brown, L. M.; Schwan, J.; Franceschini, D. F.; Marriotto, G. Nitrogen Modification of Hydrogenated Amorphous Carbon Thin Films. *J. Appl. Phys.* **1997**, *81*, 2626−2634.
(7) Dischler, B.; Bubenzer, A.; Koidl, P. Hard Carbon Coatings with Low Optical Absorption. *Appl. Phys. Lett.* **1983**, *42*, 636−638.
(8) Milne, W. I. Electronic Devices from Diamond-like Carbon. *Semicond. Sci. Technol.* **2003**, *18*, 81−85.
(9) Robertson, J. Diamond-like Amorphous Carbon. *Mater. Sci. Eng., R* **2002**, *37*, 129−281.
(10) Schwan, J.; Batori, V.; Ulrich, S.; Ehrhardt, H.; Silva, S. R. P. Nitrogen Doping of Amorphous Carbon Thin Films. *J. Appl. Phys.* **1998**, *84*, 2071−2081.
(11) Dwivedi, N.; Kumar, S.; Malik, H. K. Strange Hardness Characteristic of Hydrogenated Diamond-like Carbon Thin Film by Plasma Enhanced Chemical Vapor Deposition Process. *Appl. Phys. Lett.* **2013**, *102*, 011917.
(12) Dwivedi, N.; Kumar, S.; Malik, H. K. Superhard behaviour, Low Residual Stress and Unique Structure in Diamond-like Carbon Films by Simple Bilayer Approach. *J. Appl. Phys.* **2012**, *112*, 023518.
(13) Dwivedi, N.; Kumar, S.; Malik, H. K. Nanostructured Titanium/Diamond-like Carbon Multilayer Films: Deposition, Characterization and Applications. *ACS Appl. Mater. Interfaces* **2011**, *3*, 4268−4278.
(14) Dwivedi, N.; Kumar, S.; Tripathi, R. K.; Carey, J. D.; Malik, H. K.; Dalai, M. K. Structural and Electronic Characterization of Nanocrystalline Diamond-like Carbon Thin Films. *ACS Appl. Mater. Interfaces* **2012**, *4*, 5309−5316.
(15) Silva, S. R. P.; Amaratunga, G. A. J.; Woodburn, C. N.; Welland, M. E.; Haq, S. Quantum Size Effects in Amorphous Diamond-like Carbon Superlattices. *Jpn. J. Appl. Phys.* **1994**, *33*, 6458−6465.
(16) Davis, C. A.; Silva, S. R. P.; Borkowski, R. E. D.; Amaratunga, G. A. J.; Knowles, K. M.; Stobbs, W. M. Direct Observation of Compositionally Homogeneous a-C:H Band Gap Modulated Superlattices. *Phys. Rev. Lett.* **1995**, *75*, 4258−4261.
(17) Bhattacharyya, S.; Henley, S. J.; Mendoza, E.; Rojas, L. G.; Allam, J.; Silva, S. R. P. Resonant Tunneling and Fast Switching in Amorphous Carbon Quantum Well Structures. *Nat. Mater.* **2006**, *5*, 19−22.
(18) Dwivedi, N.; Kumar, S.; Carey, J. D.; Malik, H. K.; Govind. Photoconductivity and Characterization of Nitrogen Incorporated Hydrogenated Amorphous Carbon Thin Films. *J. Appl. Phys.* **2012**, *112*, 113706.
(19) Katkov, M. V.; Bhattacharyya, S. Enhanced Tunnel Transport in Disordered Carbon Films Incorporated with Impurities. *J. Appl. Phys.* **2012**, *111*, 123711.
(20) Fanchini, G.; Tagliaferro, A. Disorder and Urbach Energy in Hydrogenated Amorphous Carbon: A Phenomenological Model. *Appl. Phys. Lett.* **2004**, *85*, 730−732.
(21) Alibart, F.; Lejeune, M.; Drouhin, O. D.; Zellama, K.; Benlahsen, M. Influence of Disorder on Localization and Density of States in Amorphous Carbon Nitride Thin Films Systems Rich in π-Bonded Carbon Atoms. *J. Appl. Phys.* **2010**, *108*, 053504.
(22) Katkov, M. V.; McIntosh, R.; Bhattacharyya, S. Tunnel Transport Model of Nitrogen Doped Amorphous Carbon Superstructure. *J. Appl. Phys.* **2013**, *113*, 093701.
(23) Onipko, A. Analytical Model of Molecular Wire Performance: A Comparison of π and σ Electron Systems. *Phys. Rev. B: Condens. Matter Mater. Phys.* **1999**, *59*, 9995−10006.
(24) Jacobsohn, L. G.; Freire, F. L., Jr.; Franceschini, D. F.; Lacerda, M. M.; Mariotto, G. Growth Kinetics and Relationship between Structure and Mechanical Properties of a-C(N):H Films Deposited in Acetylene-Nitrogen Atmospheres. *J. Vac. Sci. Technol., A* **1999**, *17*, 545−551.
(25) Silva, S. R. P.; Amaratunga, G. A. J.; Rusli; Haq, S.; Salje, E. K. Optical Quantum Size Effects in Diamond-like Carbon Superlattice Structures. *Thin Solid Films* **1994**, *253*, 20−24.
(26) Adhikari, S.; Tian, X. M.; Adhikari, S.; Omer, A. M. M.; Uchida, H.; Umeno, M. Bonding Defects and Optical Band Gaps of DLC Films Deposited by Microwave Surface-Wave Plasma CVD. *Diamond Relat. Mater.* **2005**, *14*, 1832−1834.
(27) Wang, C.; Yang, S.; Li, H.; Zhang, J. Elastic Properties of a-C:N:HFilms. *J. Appl. Phys.* **2007**, *101*, 013501.
(28) Ferrari, A. C.; Rodil, S. E.; Robertson, J. Interpretation of Infrared and Raman Spectra of Amorphous Carbon Nitrides. *Phys. Rev. B: Condens. Matter Mater. Phys.* **2003**, *67*, 155306.
(29) Singh, S. V.; Creatore, M.; Groenen, R.; Hege, K. V.; Sanden, M. C.; M, V. D.A Hard Graphite-like Hydrogenated Amorphous Carbon grown at High Deposition Rate (> 15 nm/s). *Appl. Phys. Lett.* **2008**, *92*, 221502.
(30) Liu, S.; Gangopadhyay, S.; Sreenivas, S.; Ang, S. S.; Naseem, H. A.Infrared Studies of Hydrogenated Amorphous Carbon (a-C:H) and Its Alloys (a-C:H,N,F). *Phys. Rev. B: Condens. Matter Mater. Phys.* **1997**, *55*, 13020−13024.
(31) Dwivedi, N.; Kumar, S.; Malik, H. K.; Rauthan, C. M. S.; Panwar, O. S. Influence of Bonding Environment on Nano-mechanical Properties of Nitrogen Containing Hydrogenated Amorphous Carbon Thin Films. *Mater. Chem. Phys.* **2011**, *130*, 775−785.
(32) Kuamr, S.; Dixit, P. N.; Sarangi, D.; Bhattacharyya, R. Possible Solution to the Problem of High Built-up Stresses in Diamond-like Carbon Films. *J. Appl. Phys.* **1999**, *85*, 3866−3876.
(33) Kelires, P. C. Intrinsic Stress and Local Rigidity in Tetrahedral Amorphous Carbon. *Phys. Rev. B: Condens. Matter Mater. Phys.* **2000**, *62*, 15686−15694.
(34) McKenzie, D. R.; Muller, D.; Pailthorpe, B. A. Compressive-Stress-Induced Formation of Thin-Film Tetrahedral Amorphous Carbon. *Phys. Rev. Lett.* **1991**, *67*, 773−776.
(35) Ferrari, A. C.; Rodil, S. E.; Robertson, J.; Milne, W. I. Is Stress Necessary to Stabilise sp^3Bonding in Diamond-like Carbon? *Diamond Relat. Mater.* **2002**, *11*, 994−999.
(36) Franceschini, D. F.; Achete, C. A.; Freire, F. L., Jr. Internal Stress Reduction by Nitrogen Incorporation in Hard Amorphous Carbon Thin Films. *Appl. Phys. Lett.* **1992**, *60*, 3229−3231.
(37) Johnson, B.; Hogmark, S. Hardness Measurements of Thin Films. *Thin Solid Films* **1984**, *114*, 257−269.

DOI: 10.1021/acsami.5b05657
ACS Appl. Mater. Interfaces 2015, 7, 20726−20735

(38) Alexandrou, I.; Scheibe, H. J.; Kiely, C. J.; Papworth, A. J.; Amaratunga, G. A. J.; Schultrich, B. Carbon Films with an sp^2Network Structure. *Phys. Rev. B: Condens. Matter Mater. Phys.* **1999**, *60*, 10903−10907.
(39) Wang, C.; Yang, S.; Wang, Q.; Wang, Z.; Zhang, J. Comparative Study of Hydrogenated Diamond-like Carbon Film and Hard Hydrogenated Graphite-like Carbon Film. *J. Appl. Phys.* **2008**, *103*, 123531.
(40) Hirono, S.; Umemura, S.; Tomita, M.; Kaneko, R. Superhard Conductive Carbon NanocrystalliteFilms. *Appl. Phys. Lett.* **2002**, *80*, 425−427.
(41) Wang, Q.; Wang, C.; Wang, Z.; Zhang, J.; He, D. Fullerene Nanostructure-induced Excellent Mechanical Properties in Hydrogenated Amorphous Carbon. *Appl. Phys. Lett.* **2007**, *91*, 141902.
(42) Wang, C.; Yang, S.; Wang, Q.; Wang, Z.; Zhang, J. Super-low Friction and Super-Elastic Hydrogenated Carbon Films Originated from a Unique Fullerene-like Nanostructure. *Nanotechnology* **2008**, *19*, 225709.
(43) Hellgren, N.; Johansson, M. P.; Broitman, E.; Hultman, L.; Sundgren, J. E. Role of Nitrogen in the Formation of Hard and Elastic CN_xThin Films by Reactive Magnetron Sputtering. *Phys. Rev. B: Condens. Matter Mater. Phys.* **1999**, *59*, 5162−5169.
(44) Sjostrom, H.; Stafstrom, S.; Boman, M.; Sundgren, J. E. Superhard and Elastic Carbon Nitride Thin Films having Fullerenelike Microstructure. *Phys. Rev. Lett.* **1995**, *75*, 1336−1339.
(45) Stafstrom, S. Reactivity of Curved and Planar Carbon Nitride Structures. *Appl. Phys. Lett.* **2000**, *77*, 3941−3943.
(46) Liu, A. Y.; Cohen, M. L. Prediction of New Low Compressibility Solids. *Science* **1989**, *245*, 841−842.
(47) Liu, A. Y.; Wentzcovitch, R. M. Stability of Carbon Nitride Solids. *Phys. Rev. B: Condens. Matter Mater. Phys.* **1994**, *50*, 10362−10365.
(48) Ren, Z. M.; Du, Y. C.; Qiu, Y.; Wu, J. D.; Ying, Z. F.; Xiong, X. X.; Li, F. M. Carbon Nitride Films Synthesized by Combined Ion-Beam and Laser-Ablation Processing. *Phys. Rev. B: Condens. Matter Mater. Phys.* **1995**, *51*, 5274−5277.
(49) Keay, B. J.; Allen, S. J., Jr.; Galan, J.; Kaminski, J. P.; Campman, K. L.; Gossard, A. C.; Bhattacharyya, U.; Rodwell, M. J. W. Photon-Assisted Electric Field Domains and Multiphoton-Assisted Tunneling in Semiconductor Superlattices. *Phys. Rev. Lett.* **1995**, *75*, 4098−4101.
(50) Bhattacharyya, S.; Silva, S. R. P. Demonstration of an Amorphous Carbon Tunnel Diode. *Appl. Phys. Lett.* **2007**, *90*, 082105.

DOI: 10.1021/acsami.5b05657
ACS Appl. Mater. Interfaces 2015, 7, 20726−20735